The spatial logistic map as a simple prototype for spatiotemporal chaos

Article *in* Chaos · July 2003

DOI: 10.1063/1.1568692 · Source: PubMed

1 author:

Frederick H. Willeboordse

44 PUBLICATIONS **731** CITATIONS

SEE PROFILE

The spatial logistic map as a simple prototype for spatiotemporal chaos

Frederick H. Willeboordse[a)]
Department of Physics, The National University of Singapore, Singapore 119260, Singapore

(Received 24 October 2002; accepted 28 February 2003; published 8 May 2003)

A spatial extension of the logistic map—termed spatial logistic map—is found to display the same basic universality classes as the commonly studied diffusively coupled logistic lattice despite being vastly simpler. By analyzing the escape rates and the Lyapunov spectra it is shown that the main attractors of the spatial logistic map are stable and hence that it is a good candidate for serving as a prototype for the class of coupled map lattices which it is a part of. The spatial logistic map is then employed to provide an analytical derivation for the recently discovered linear scaling of the wavelength under increasing coupling ranges. © *2003 American Institute of Physics.*
[DOI: 10.1063/1.1568692]

Coupled map lattices are studied widely as computationally efficient examples of high dimensional chaotic systems. A key motivation is the search for universal properties and behaviors that apply to entire classes of systems. One such property that was found to exist in many one-dimensional coupled map lattices is a certain sequence in the main types of patterns. This sequence, termed the basic pattern sequence here, occurs when increasing the nonlinearity. In this article, a spatial logistic map is introduced that appears to be the simplest map with a continuous state displaying the basic pattern sequence. It can therefore serve as a prototype for this class of systems and make the analysis of its dynamics significantly easier. As a concrete application, the spatial logistic map is employed to analytically prove the linear scaling of the spatial periodicity, i.e., the wavelength, in one of the basic patterns versus the coupling range by renormalization.

I. INTRODUCTION

In the study of higher dimensional chaos, coupled map lattices have played an important role as paradigms for a wide variety of fascinating phenomena like pattern selection and traveling waves in the diffusively coupled logistic lattice or clustering the globally coupled logistic lattice.[1–15] Recently, it was found that many coupled map lattices share a common sequence of major patterns, regardless of the local map or its power and it was also found that in all those cases the patterns scale linearly with the coupling range.[16]

It is therefore interesting to investigate what the simplest coupled map lattice is that displays these properties. In this paper, it will be shown that the spatial logistic map (which reduces to the single logistic map in the case of a homogeneous lattice), defined as

$$x_{n+1}^{i}=1.0-\frac{\alpha}{2}x_n^i(x_n^{i-1}+x_n^{i+1}), \tag{1}$$

is probably the simplest coupled map lattice that displays the basic pattern sequence (some justification for calling it ''probably the simplest'' is given in the Appendix). The simplicity of Eq. (1) facilitates mathematical analysis and a basic proof of the above-mentioned linear scaling is given in Sec. IV. It is expected that this proof is also applicable to other systems that fall into the same universality class.

The basic pattern sequence for the spatial logistic map Eq. (1) is shown in Fig. 1 and found to be identical to the pattern sequence of the diffusively coupled logistic lattice. However, contrary to the single logistic map, Eq. (1) is not bound to $[-1,1]$ when starting from random initial conditions in this interval, and a trajectory can escape to infinity. Detailed escape rates are investigated in Sec. II but Figs. 1(a)–1(c) can easily be obtained by starting from random initial conditions $x_0^i \in [0.0,1.0]$. As can be expected, for larger values of the nonlinearity α, the tendency to escape increases and hence, in order to obtain the supertransient spatio-temporal chaos depicted in Fig. 1(d), a value of α was chosen such that the single logistic map is near the $2\rightarrow 1$ band merging point. The lattice can then be forced onto a two-band attractor corresponding to the one-band supertransient attractor at higher nonlinearities by limiting the amplitude of the random initial conditions.[17] In this case, the initial conditions were chosen such that: $x_0^i \in [-0.1,0.1]$.

In the same way as for the diffusively coupled logistic lattice, the spatial logistic map can straightforwardly be extended to longer coupling ranges:

$$x_{n+1}^{i}=1.0-\frac{\alpha}{2r}x_n^i\sum_{k=1}^{k=r}(x_n^{i-k}+x_n^{i+k}). \tag{2}$$

The coupling range then becomes an additional parameter that can have a significant impact on the dynamics of the system yielding in the extreme case of $r=N/2$ a globally coupled lattice [setting $r=N/2$ in Eq. (2) always seems to lead to a spatially homogeneous solution and consequently it cannot serve as a prototype for globally coupled maps].

When the coupling range is not near the extreme case of $r=N/2$, its effect is a (linear) scaling in the spatial structures of the attractors. This is illustrated in Fig. 2 where the pattern selection attractor is shown for several values of the coupling

a)Electronic mail: willeboordse@yahoo.com

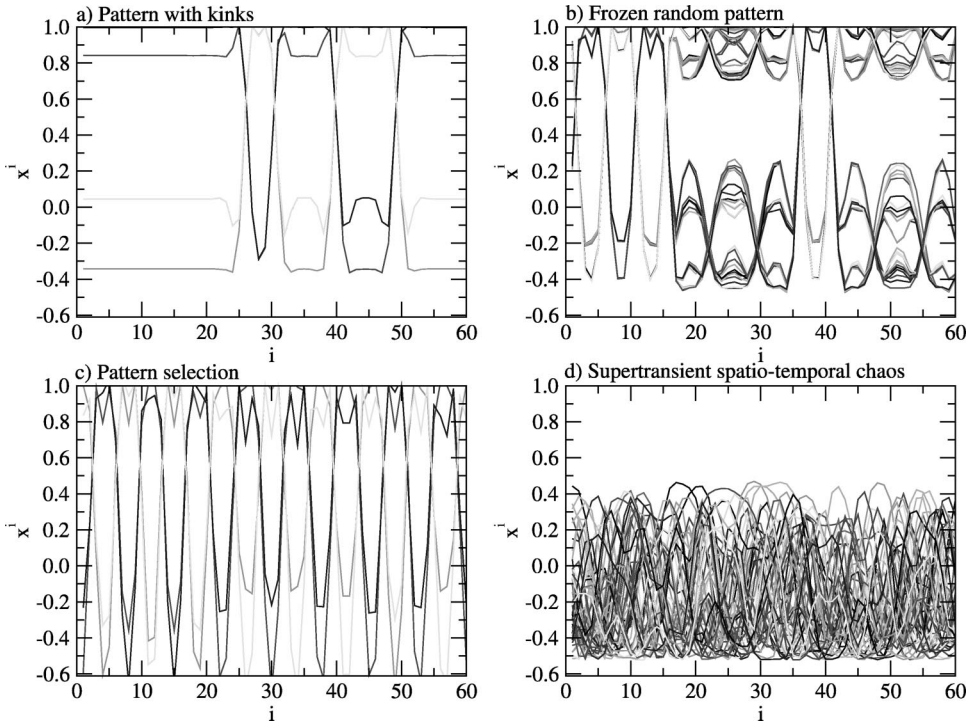

FIG. 1. The basic pattern sequence of the spatial logistic map Eq. (1). (a) Pattern with kinks, $\alpha=1.35$, (b) frozen random pattern, $\alpha=1.45$, (c) pattern selection, $\alpha=1.7$, (d) supertransient spatiotemporal chaos, $\alpha=1.52$. The panes depict 50 successive states of the lattice after a transient of 10^5 time steps was discarded starting from different sets of random initial conditions where $x_0^i \in [0.0,1.0]$ for (a), (b), and (c), and $x_0^i \in [-0.1,0.1]$ for (d). Periodic boundary conditions are used throughout this paper.

range (the scaling behavior is analyzed in more detail in Sec. IV). Even though the patterns are very similar, they are not exactly the same. This is due to the fact that in most cases, the pattern selection attractor has four temporal phases which can succeed each other spatially [this can also be seen in Fig. 1(c)]. That is to say, a spatial pulse consisting of the neighboring sites that form the pulse in the wave-like pattern is temporally period four but even though there is only one type of such a pulse in the attractor, successive spatial segments of the lattice can be attracted to any of the phases of this pulse leading to the slight differences in the patterns.[18] Furthermore, since the lattice size was kept constant, the amount of frustration can change for each of the coupling ranges leading to some additional differences.

II. ESCAPE RATES

Even though the spatial logistic map Eq. (1) clearly can escape to infinity, the escape rate will depend on the system size, the nonlinearity, and the maximum amplitude of the

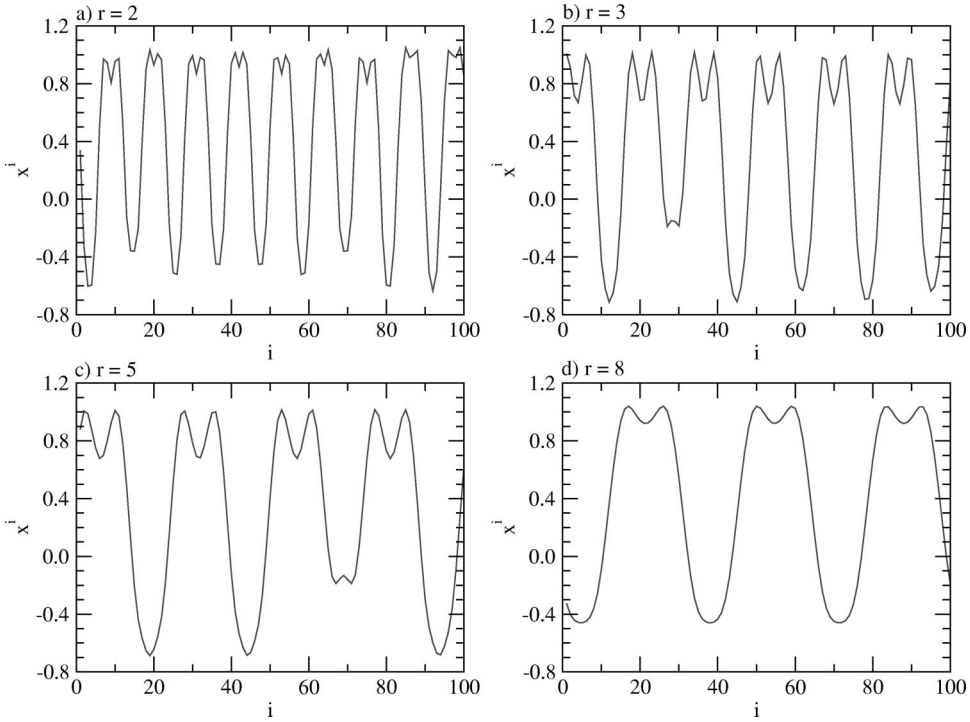

FIG. 2. Wavelength scaling in the pattern selection regime of Eq. (2). The nonlinearity is $\alpha=1.7$ and the coupling ranges are: (a) $r=2$, (b) $r=3$, (c) $r=5$, (d) $r=8$. All patterns were obtained by starting from positive random initial conditions between 0 and 1. The increase in the spatial periodicity, i.e., the wavelength, can clearly be seen.

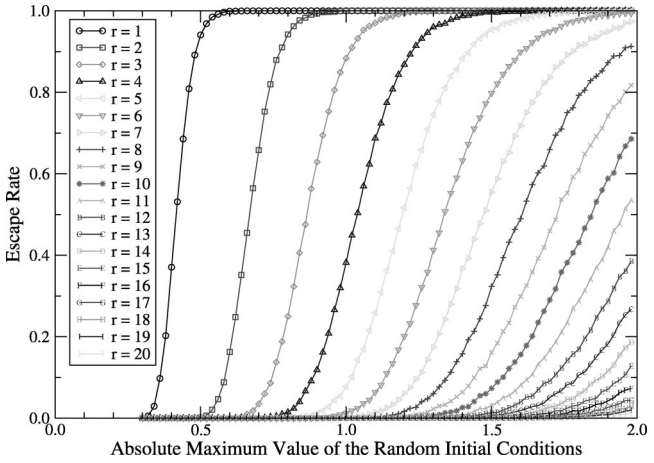

FIG. 3. Escape rates vs the maximum amplitude b of the random initial conditions for coupling ranges from $r=1$ to $r=20$ such that $x_0^i \in [-b,b]$. The nonlinearity is $\alpha=1.7$ and the system size is $N=200$.

random initial conditions. In this section, it shall be shown that while when starting from regular random initial conditions escaping trajectories can be frequent for larger values of the nonlinearity, this is not the case for smaller values of the nonlinearity. By employing amplitude limited random initial conditions, the full range of basic patterns can be obtained without escaping trajectories. This is important in order for the spatial logistic map to be useful as a prototype for this class of coupled map lattices. In Fig. 3, the escape rates for coupling ranges $r=1$ to $r=20$ are plotted versus the maximum amplitude of the random initial conditions [i.e., if the maximum amplitude is 0.0, the initial conditions are homogeneous and Eq. (1) is reduced to the single logistic map].

For each data point, $10E5$ trajectories were followed and considered as an escaping trajectory if the absolute value of any lattice point becomes larger than 10 within 100 time steps. Otherwise the trajectory was considered to be bound. The cutoff value of 10 is arbitrary but must be sufficiently large in order for the maximum investigated coupling range (20 in this figure) to have a negligible probability of ''pulling back'' the trajectory of a lattice where one site has passed this threshold. For the nonlinearity, system size, and coupling range used in this figure, when not escaping to infinity, the lattice will be attracted to a stable wave-like pattern. Once the lattice has reached this stable attractor, no spontaneous escapes to infinity have been observed (contrary to the higher nonlinearity supertransient spatiotemporally chaotic case). Hence it is only necessary to follow the trajectory for a short time. As can be seen in Fig. 4(b), most trajectories will cross the threshold after around 4–6 time steps although a trajectory can in principle escape anytime during the transient (i.e., before reaching a stable attractor).

It can be expected that the nonzero escape rates depend on the system size as can be seen in Figs. 4(a) and 4(c). The maximum amplitude of the initial conditions was the standard 1.0 and although for longer coupling ranges the escape rate can be very small, no nonzero escape rates were found for this value of the nonlinearity.

In general, the initial stages of the escape are not a global but a local phenomenon. That is to say, escape is due to a certain combination of neighboring lattice sites within a range in the order of several r. Consequently, as long as there is a finite escape rate, there will not be an infinite size limit since the combination of neighboring sites that leads to escape is certain to occur somewhere for a sufficiently large lattice.

For smaller values of the nonlinearity, the situation is rather different as can be seen in Fig. 5 which depicts the escape rates versus the maximum amplitude for $\alpha=1.46$ and $\alpha=1.7$ for comparison.

The important qualitative difference between the $\alpha=1.7$ and $\alpha=1.46$ cases is that for small (nonzero) maximum amplitudes some trajectories will still escape when $\alpha=1.7$ but

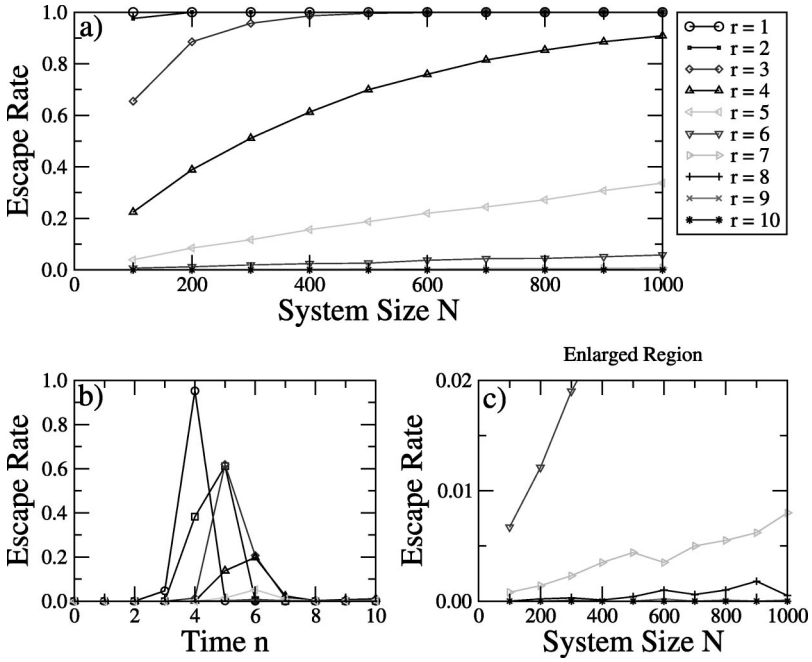

FIG. 4. (a) The escape rate vs N for $\alpha=1.7$, (b) the escape rate vs time for a system size of $N=200$, and (c) an enlarged part of (a) for small escape rates where the rates for longer coupling ranges are better visible. Except for the maximum amplitude of the random initial conditions which was set to 1.0 and the number of time steps the trajectory was followed (set to $10E5$), the escape rates were determined in the same way as in Fig. 3.

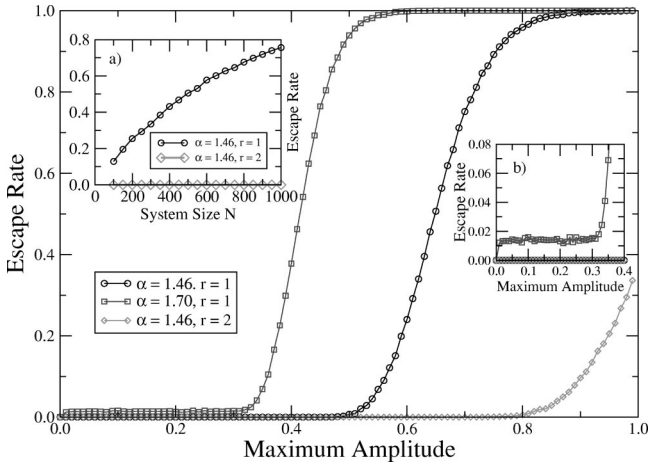

FIG. 5. Escape rate vs the absolute maximum value of the random initial conditions. (a) The escape rate vs the system size for a maximum amplitude of the random initial conditions of 0.6. (b) Zooms in on the region near the origin so that the nonzero escape rate for $\alpha=1.7$ can clearly be seen. The escape rates were determined in the same way as in Fig. 3 but the trajectory was followed for $10E5$ time steps rather than for 100 time steps in order to clearly obtain the nonzero escape rate for small maximum amplitudes in the case of $\alpha=1.7$.

not when $\alpha=1.46$. Consequently, for $\alpha=1.46$, a nonescaping infinite size limit should exist.

This appears to be due to the range of possible initial conditions not being large enough to allow for escaping sets when the nonlinearity is such that the single logistic map has chaotic bands and the initial conditions are chosen to fall within one of these chaotic bands (some more details are provided in the Appendix).

III. LYAPUNOV SPECTRA

Lyapunov exponents provide an important quantitative measure for the stability of a chaotic system. For spatially extended systems, Lyapunov spectra can be determined analogously to one-dimensional systems by replacing the derivatives by Jacobi matrices and by calculating the eigenvalues of their products.[19–21] The ith Lyapunov exponent is obtained as

$$\lambda_i=\lim_{n\to\infty}\frac{1}{n}\ln[\,i\text{th eigenvalue of }(J_{n-1}J_{n-2}\ldots J_0)], \tag{3}$$

where the Jacobi matrix at time n is given by

$$(J_n)_{i,j}=\frac{\partial x_{n+1}^i}{\partial x_n^j}. \tag{4}$$

For N-dimensional maps there are N Lyapunov exponents and since expansion or contraction can occur along any of the axes, their labeling is arbitrary. Consequently, the exponents are usually ordered from large to small. In the case of the spatial logistic map Eq. (2), the Jacobi matrix for $r=2$ at time n is, for example, given by

$$J_n=-\frac{\alpha}{2r}\begin{pmatrix}
\sum_{1,2,n}' & x_n^1 & x_n^1 & 0 & 0 & \cdots & 0 & 0 & x_n^1 & x_n^1\\
x_n^2 & \sum_{2,2,n}' & x_n^2 & x_n^2 & 0 & 0 & \cdots & 0 & 0 & x_n^2\\
x_n^3 & x_n^3 & \sum_{3,2,n}' & x_n^3 & x_n^3 & 0 & 0 & \cdots & 0 & 0\\
0 & x_n^4 & x_n^4 & \sum_{4,2,n}' & x_n^4 & x_n^4 & 0 & 0 & \cdots & 0\\
\vdots & & \varnothing & & & \ddots & & \varnothing & & \vdots\\
0 & \cdots & 0 & 0 & x_n^{N-3} & x_n^{N-3} & \sum_{N-3,2,n}' & x_n^{N-3} & x_n^{N-3} & 0\\
0 & 0 & \cdots & 0 & 0 & x_n^{N-2} & x_n^{N-2} & \sum_{N-2,2,n}' & x_n^{N-2} & x_n^{N-2}\\
x_n^{N-1} & 0 & 0 & \cdots & 0 & 0 & x_n^{N-1} & x_n^{N-1} & \sum_{N-1,2,n}' & x_n^{N-1}\\
x_n^N & x_n^N & 0 & 0 & \cdots & 0 & 0 & x_n^N & x_n^N & \sum_{N,2,n}'
\end{pmatrix}, \tag{5}$$

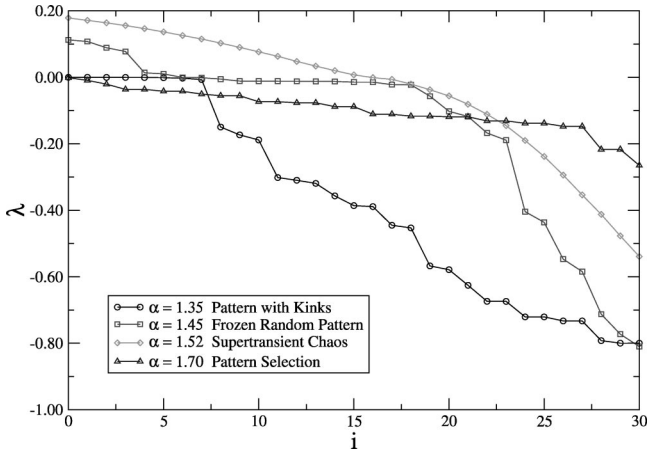

FIG. 6. The Lyapunov spectra for the basic patterns depicted in Fig. 1. All the parameters were identical to those of Fig. 1. Only the largest 30 Lyapunov exponents are shown. The system size was set to $N=60$.

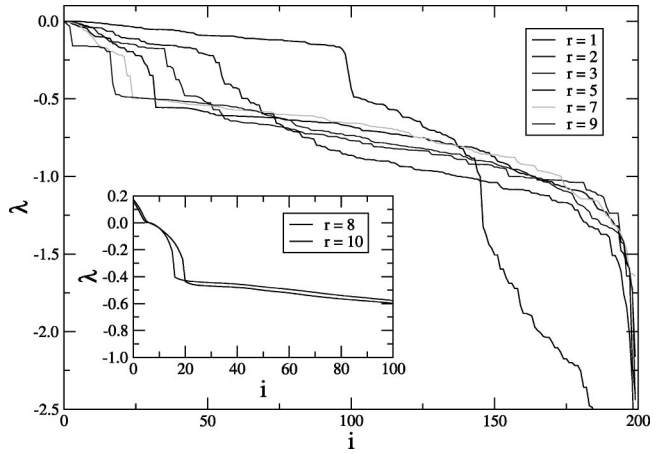

FIG. 7. Lyapunov spectra for various coupling ranges in a lattice with a fixed size $N=200$. The inset shows the largest 100 exponents of the strongly frustrated $r=8$ and $r=10$ cases. The nonlinearity $\alpha=1.7$.

where the sum of the neighbors is defined as

$$\sum_{l,r,n}{}' = \sum_{k=1}^{k=r} (x_n^{i-k} + x_n^{i+k}). \tag{6}$$

Figure 6 shows the Lyapunov spectra for the basic patterns of Fig. 1. For all the spectra in this paper, the product of $10E5$ Jacobi matrices was taken after a transient of $10E6$ time steps. If a pattern turned out to be of the traveling-wave type, the computation was reset in order to assure that comparisons between the spectra are on the same basis. Qualitatively, the spectra are identical to those of the diffusively coupled logistic lattice providing further confirmation of the phenomenological similarity between the systems.

The spectrum for patterns with kinks consists only of negative Lyapunov exponents consistent with the periodic nature of the homogeneous solution for the same value of the nonlinearity. While the pattern selection attractor is basically periodic in time and space, which would imply a completely negative Lyapunov spectrum, in many cases, the attractor contains sites that display remnant (or possibly very-long/supertransient) chaotic behavior that leads to some slightly positive exponents in the spectrum. The remaining exponents, however, are clearly negative. Consequently, the pattern is stable and therefore cannot escape to infinity after reaching this state. Not surprisingly, the spectrum for the frozen random pattern consists of two parts connected by a range of near zero exponents. Since the spatial structure and hence sizes of the regular and chaotic (or supertransient) regions of the frozen random pattern strongly depend on the initial conditions, this range of near zero exponents can vary quite substantially unless the system size is very large. The part with the positive exponents is smooth, similar to the case for (supertransient) spatiotemporal chaos, and the part with the negative exponents stepwise like the case for pattern selection. Lastly, the spectrum for (supertransient) fully developed spatiotemporal chaos consists of a smooth top of a finite fraction of clearly positive Lyapunov exponents and a tail of negative Lyapunov exponents. The ratio of positive Lyapunov exponents is around 1/3, which is about the same as in the case of the diffusively coupled logistic lattice for $\alpha=1.9$ and $\epsilon=0.5$.[5]

Figure 7 depicts the Lyapunov spectra of the pattern selection attractor for various coupling ranges in a lattice with a fixed system size. As can be seen, all the spectra display the characteristic initial stepwise decline from larger to smaller Lyapunov exponents followed by a long smoothly declining tail. The key feature is that for increasing coupling ranges, the beginning of the tail moves toward the left in the Fig. 7 indicating the expected increased stability for larger r. Given a fixed lattice size, for sufficiently large r, the system can experience severe frustration. This was observed for $r=8$ and $r=10$ and its effects are shown in the inset of Fig. 7. While overall, the pattern is wavelike without displaying defects, there is strong remnant chaos leading to chaotic itinerancy. This remnant chaos is reflected in the smooth arc of positive Lyapunov exponents.

Lastly, it was investigated how the Lyapunov spectrum of the pattern selection attractor scales when the number of pulses is kept fixed. The result is shown in Fig. 8. The lattice sizes were chosen such that exactly ten pulses fit for a given coupling range and determined by using the linear relationship obtained in Fig. 9. As clearly can be seen, the index i of the Lyapunov exponent where the roughly stepwise decline changes to a smooth tail is basically identical in all three cases and hence a consequence of the number of pulses and not of the system size or the coupling range as such.

IV. SCALING BEHAVIOR

Previously, it was found that the wavelengths in the pattern selection regime scale linearly when increasing the coupling range.[16] This also turns out to be the case for Eq. (2) as can be seen in Fig. 9.

The relative simplicity of the spatial logistic map makes the analysis of this scaling behavior much easier and it is found that it can be understood by considering the sum of two neighboring lattice sites and by rescaling the resulting equation.

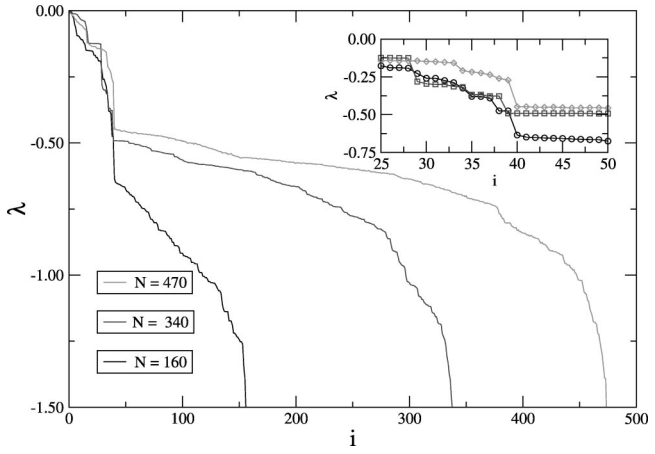

FIG. 8. Lyapunov spectra for various coupling ranges for a fixed number of pulses (10). For $r=3$, $N=160$; for $r=7$, $N=340$; for $r=10$, $N=470$. The inset is an enlargement of the region where the stepwise head connects to the smooth tail.

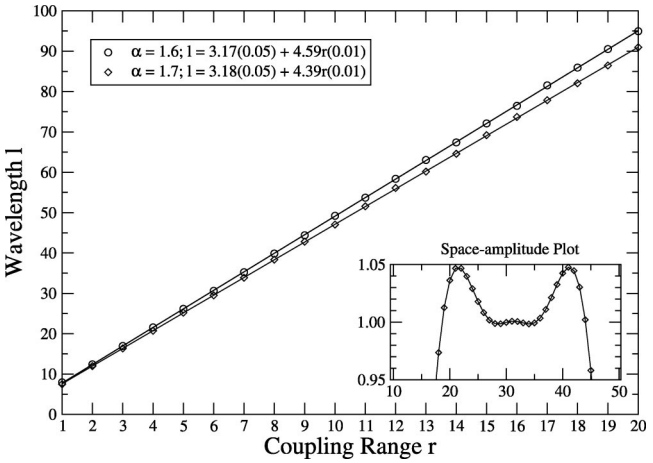

FIG. 9. The wavelength scales linearly with the coupling range. The symbols represent the computationally obtained data points while the lines are the result of linear regression. The inset shows part of a lattice with a system size of $N=200$, a nonlinearity of $\alpha=1.7$, and a coupling range of $r=15$. Some lattice sites clearly exceed $x=1$, the repellor of the uncoupled system.

Adding two neighboring sites in Eq. (2) yields

$$\frac{x_{n+1}^{i}+x_{n+1}^{i+1}}{2}=1-\left(\frac{x_{n}^{i}+x_{n}^{i+1}}{2}\right)\sum_{i,r,n}-S_{i,r,n}, \tag{7}$$

where

$$\sum_{i,r,n}\equiv\frac{\alpha}{2r}\sum_{k=1}^{r}(x_{n}^{i-k}+x_{n}^{i+1+k}) \tag{8}$$

and

$$S_{i,r,n}\equiv\frac{\alpha}{4r}[(x_{n}^{i+1}-x_{n}^{i+1+r})x_{n}^{i}+(x_{n}^{i}-x_{n}^{i-r})x_{n}^{i+1}]. \tag{9}$$

For very large coupling ranges, $S_{i,r,n}$ will be negligibly small and Eq. (7) can be rescaled by substituting $z_i=(x_i+x_{i+1})/2$, changing the spatial index to $j=i/2$ and the coupling range to $r'=1/2r$. Hence, for very large coupling ranges, the linear scaling is obvious immediately.

Numerically (Fig. 9), it is found, however, that the linear scaling not only occurs for very large coupling ranges but for all coupling ranges.

Clearly term (9) cannot directly be rescaled due to the cross products. By considering higher iterates, however, it can be expressed in terms of rescalable sums of the form (8).

Since the products on the right-hand side of term (9) are identical as with regards to their structure, it is sufficient to consider only one of them. Inserting [i.e., Eq. (2) at time n]

$$x_{n}^{i}=1-x_{n-1}^{i}\sum_{i,r,n-1}-S_{i,r,n-1}^{I}, \tag{10}$$

into

$$S_{i,r,n}^{I}\equiv\frac{\alpha}{2r}(x_{n}^{i+1}-x_{n}^{i+1+r})x_{n}^{i}, \tag{11}$$

yields

$$\begin{aligned}S_{i,r,n}^{I}=\frac{\alpha}{2r}\Bigg[&-x_{n-1}^{i+1}\sum_{i+1,r,n-1}-S_{i+1,r,n-1}^{I}+x_{n-1}^{i+1+r}\sum_{i+1+r,r,n-1}+S_{i+1+r,r,n-1}^{I}+x_{n-1}^{i+1}x_{n-1}^{i}\sum_{i,r,n-1}\sum_{i+1,r,n-1}\\&+x_{n-1}^{i}\sum_{i,r,n-1}S_{i+1,r,n-1}^{I}-x_{n-1}^{i+1+r}x_{n-1}^{i}\sum_{i,r,n-1}\sum_{i+1+r,r,n-1}-x_{n-1}^{i}\sum_{i,r,n-1}S_{i+1+r,r,n-1}^{I}+x_{n-1}^{i+1}\sum_{i+1,r,n-1}S_{i,r,n-1}^{I}\\&+S_{i,r,n-1}^{I}S_{i+1,r,n-1}^{I}-x_{n-1}^{i+1+r}\sum_{i+1+r,r,n-1}S_{i,r,n-1}^{I}-S_{i,r,n-1}^{I}S_{i+1+r,r,n-1}^{I}\Bigg]\end{aligned} \tag{12}$$

which clearly has three types of terms:

$$\text{I:}\quad x_{n}^{i}\frac{\alpha}{2r}\sum_{i,r,n}, \tag{13}$$

$$\text{II:}\quad x_{n}^{i}\frac{\alpha}{2r}\sum_{i,r,n}S_{i+k,r,n}^{I}, \tag{14}$$

$$\text{III:}\quad \frac{\alpha}{2r}S_{i,r,n}^{I} \tag{15}$$

with k an integer.

When iterating Eq. (12) further, at each step, type III terms gain a factor $\alpha/2r$, which implies that they go to zero since $\alpha/2r<1$ and hence can be ignored. Similarly, for

higher iterates, term II will either contain $S^I_{i,r,n}$ terms, which will again go to zero due to the factor $\alpha/2r$, or be composed of type I terms. Consequently, the only term relevant as with regards to rescaling is term I. Iterating term I one more time by inserting Eq. (10) yields

$$x^i_n \frac{\alpha}{2r}\sum_{i,r,n} = \left(1 - x^i_{n-1}\sum_{i,r,n-1} - S^I_{i,r,n-1}\right)\frac{\alpha}{2r}\sum_{i,r,n}$$

$$= \frac{\alpha}{2r}\sum_{i,r,n} - x^i_{n-1}\frac{\alpha}{2r}\sum_{i,r,n-1}\sum_{i,r,n}$$

$$- S^I_{i,r,n-1}\frac{\alpha}{2r}\sum_{i,r,n}. \quad (16)$$

The right-hand side of Eq. (16) again contains three terms. The first of these, $(\alpha/2r)\Sigma_{i,r,n}$, is rescalable and hence does not need any further consideration, the third term, $S^I_{i,r,n-1}(\alpha/2r)\Sigma_{i,r,n}$, is the product of the rescalable $\Sigma_{i,r,n}$ and term III and hence does not need further consideration either.

This leaves the middle term $x^i_{n-1}(\alpha/2r)\Sigma_{i,r,n-1}\Sigma_{i,r,n}$ which, when iterating Eq. (16), will lead to a product of sums $\Sigma_{i,r,n}$ as

$$x^i_n \frac{\alpha}{2r}\sum_{i,r,n} = x^i_{n-k}\frac{\alpha}{2r}\sum_{i,r,n-k}\sum_{i,r,n-k+1}\cdots\sum_{i,r,n}$$

$$+ \text{other terms that go to zero.} \quad (17)$$

Since the wave-type solutions are temporally periodic, $x^i_n = x^i_{n-k}$ when k equals the temporal periodicity and hence x^i_n can be divided out leaving only rescalable $\Sigma_{i,r,n}$ type terms.

For sufficiently high iterates, Eq. (2) can therefore entirely be expressed as either the sum of rescalable terms or of terms that will go to zero under iteration. Consequently, the spatial logistic map scales linearly even at short coupling ranges. Naturally, for smaller system sizes, this rescalability can be distorted due to finite size effects.

V. CONCLUSION

When iterating coupled map lattices, the number of terms increases very rapidly and it is therefore of significant value to identify the simplest possible map that displays certain characteristic dynamical behaviors. This map can then serve as a prototype for the class of dynamical systems with the same characteristics. In this paper, it is shown that the spatial logistic map is quite suitable as a prototype for the class of systems often represented by the nearest neighbor diffusively coupled logistic lattice. As an application, a previously discovered linear dependence of the wavelength on the coupling range was investigated analytically and a proof for this dependence given that employs far fewer terms than otherwise would have been required if the standard diffusively coupled logistic lattice would have been used.

APPENDIX: SIMPLICITY

In its usual definition, the diffusively coupled logistic lattice when extended to larger coupling ranges[16] is given by

$$x^i_{n+1} = (1-\varepsilon)f(x^i_n) + \frac{\varepsilon}{2r}\sum_{k=1}^{r}\left(f(x^{i-k}_n) + f(x^{i+k}_n)\right), \quad (A1)$$

where $f(x)$ is the single logistic map $f(x_n) = x_{n+1} = 1 - \alpha x^2_n$ with α the nonlinearity, ε the coupling constant, and r the coupling range. The subscript n and the superscript i denote the (discrete) time and space, respectively. When comparing this to the spatial logistic map Eq. (2), it may appear that a summation is replaced by a possibly more complicated albeit shorter multiplication. This is not the case, however, since the sequence of coupling and mapping in the diffusively coupled logistic lattice are arbitrary as can be seen by applying f to both sides and substituting $x' = f(x)$. When coupling first and mapping second, after explicit application of f, the diffusively coupled logistic lattice becomes

$$x^i_{n+1} = 1 - \frac{\alpha}{4}x^{i\,2}_n - \frac{\alpha}{4r}x^i_n\sum_{n,i} - \frac{1}{4r^2}\sum_{n,i}^{2}, \quad (A2)$$

with $\Sigma_{n,i} = \Sigma^{-1}_{j=-r}\, x^{i+j}_n + \Sigma^{r}_{j=1}\, x^{i+j}_n$. When comparing Eq. (A2) to Eq. (2), it can be seen that in essence, the right hand side of the spatial logistic map Eq. (2) is comprised of right-hand side terms 1 and 3 of the diffusively coupled logistic lattice Eq. (A2). In other words, aside from a factor 2 that does not affect the structure of the terms, the diffusively coupled logistic lattice equals the spatial logistic map plus extra terms. Hence the spatial logistic map is vastly simpler in this respect than the diffusively coupled logistic map, especially when considering higher iterates.

To a certain extent, the possibility of escapes to infinity equates some loss in simplicity as compared to the diffusively coupled logistic map that is bound when $\alpha \in [0,2]$, $\varepsilon \in [0,1]$ and $x_0 \in [-1,1]$. The main dynamics of the diffusively coupled logistic lattice are however repeated at smaller scales (albeit at higher periodicities) in the chaotic bands if suitable amplitude limited random initial conditions are used.[17,22] For example, the basic pattern sequence can be found for $\alpha \in [0.75$ (first bifurcation),1.54 ($2 \to 1$ band-merging point)] if the (otherwise random) initial conditions are, e.g., $x^i_0 \in [0.5,1]$. Limiting the initial conditions to bands naturally also limits the possible combinations that can lead to escape and indeed, it was numerically confirmed that for $\alpha = 1.45$ an interval can be found for which all initial conditions in this interval map to a point within the interval itself. This was done by considering the second iterate of Eq. (1),

$$x^i_{n+2} = 1 - \frac{\alpha}{2}\left[1 - \frac{\alpha}{2}x^i_n x^{i-1}_n - \frac{\alpha}{2}x^i_n x^{i+1}_n\right]\left[1 - \frac{\alpha}{2}x^{i-1}_n x^{i-2}_n\right.$$

$$\left. - \frac{\alpha}{2}x^{i-1}_n x^i_n + 1 - \frac{\alpha}{2}x^{i+1}_n x^i_n - \frac{\alpha}{2}x^{i+1}_n x^{i+2}_n\right] \quad (A3)$$

and looping through all possible combinations of $x^{i-2}_n \cdots x^{i+2}_n$ with steps sized 0.001. It was found that when $x_n \in [0.62,1.03]$, $x_{n+2} \in [0.662\,65,1.016\,62]$.

While the connection of the spatial logistic map to the diffusively coupled map lattice is in a sense twofold in that it is identical in the case of the homogeneous lattice and shares the cross term otherwise, there seems to be no straightfor-

ward way to apply this approach to local maps like the circle map even though the dynamics of the coupled lattice shows significant similarities. It may be interesting for future research to investigate in more detail what terms play a key role in the common dynamics.

[1] J. P. Crutchfield and K. Kaneko, *Directions in Chaos* (World Scientific, Singapore, 1987).
[2] K. Kaneko, Prog. Theor. Phys. **72**, 480 (1984).
[3] K. Kaneko, Physica D **34**, 1 (1989).
[4] K. Kaneko, Physica D **77**, 456 (1994).
[5] F. H. Willeboordse, Phys. Rev. E **47**, 1419 (1993).
[6] K. Konishi, H. Kokame, and K. Hirata, Phys. Rev. E **62**, 6383 (2000).
[7] Y. Kuramoto and H. Nakao, Phys. Rev. Lett. **76**, 4352 (1996).
[8] N. B. Ouchi and K. Kaneko, Chaos **10**, 359 (2000).
[9] S. P. Kuznetsov and E. Mosekilde, Physica A **291**, 299 (2001).
[10] S. P. Kuznetsov, in *Theory and Applications of Coupled Map Lattices*, edited by K. Kaneko (Wiley, New York, 1993), p. 50.
[11] A. Crisanti, M. Falcioni, and A. Vulpiani, Phys. Rev. Lett. **76**, 612 (1996).
[12] A. Pikovsky, M. Rosenblum, and J. Kurths, Europhys. Lett. **34**, 165 (1996).
[13] A. Pikovsky and J. Kurths, Physica D **76**, 411 (1994).
[14] O. Popovych, A. Pikovsky, and Y. Maistrenko, Physica D **168**, 106 (2002).
[15] F. H. Willeboordse and K. Kaneko, Phys. Rev. Lett. **73**, 533 (1994).
[16] F. H. Willeboordse, Phys. Rev. E **65**, 026202 (2002).
[17] F. H. Willeboordse, Chaos, Solitons Fractals **2**, 609 (1992).
[18] F. H. Willeboordse, Int. J. Bifurcation Chaos Appl. Sci. Eng. **2**, 721 (1992).
[19] I. Shimada and T. Nagashima, Prog. Theor. Phys. **61**, 1605 (1979).
[20] R. Deissler and K. Kaneko, Phys. Lett. A **119**, 397 (1987).
[21] S. Isola, A. Politi, S. Ruffo, and A. Torcini, Phys. Lett. A **143**, 365 (1990).
[22] F. H. Willeboordse, Phys. Lett. A **183**, 187 (1993).